Use of periodic approximants in a dynamical LEED study of the quasicrystalline tenfold surface of decagonal Al-Ni-Co

K. Pussi

Department of Electrical Engineering, Lappeenranta University of Technology, P.O. Box 20, FIN-53851 Lappeenranta, Finland

N. Ferralis

Physics Department and Materials Research Institute, Penn State University, University Park, Pennsylvania 16802, USA

M. Mihalkovic

Slovak Academy of Sciences, Dubravska Cesta 9, Bratislava 84228, Slovakia

M. Widom

Department of Physics, Carnegie Mellon University, Pittsburgh, Pennsylvania 15213, USA

S. Curtarolo

Department of Materials Science and Mechanical Engineering, Duke University, Durham, North Carolina 27708, USA

M. Gierer

Institute for Crystallography and Applied Mineralogy, Theresienstrasse 41, 80333 München, Germany

C. J. Jenks, P. Canfield, and I. R. Fisher*

Ames Laboratory, Iowa State University, Ames, Iowa 50011, USA

R. D. Diehl

Physics Department and Materials Research Institute, Penn State University, University Park, Pennsylvania 16802, USA

The determination of quasicrystal (QC) surface structures is a challenge to current surface structure techniques. Low-energy electron diffraction (LEED) is the primary technique for the determination of periodic surface structures, but application of dynamical LEED to quasicrystals requires the use of many approximations. In this study, two different approaches were used to apply dynamical LEED to the structure of the tenfold surface of decagonal $Al_{73}Ni_{10}Co_{17}$. One method (method 1) involves the use of a quasicrystalline model along with approximations that average over the composition and local geometries. The other method (method 2) uses periodic models that approximate the actual local QC structure (approximants) in more exact, atomistic calculations. Although the results using the two methods were consistent, the results of the approximant analysis (method 2) suggested a different way to apply the approximations in method 1, resulting in a better fit between experimental and calculated beams. Thus, periodic approximant structure models can provide a simpler and more efficient method for the determination of local geometries in QC surfaces, and may also facilitate analyses using quasicrystal models.

INTRODUCTION

Because of the growing interest in using quasicrystalline (QC) substrates as templates for producing quasicrystalline overlayers or nano-ordered arrays having quasicrystalline order,[1] the characterization of the structure, morphology, and composition of the surfaces is very important. Low-energy electron diffraction (LEED) is a primary technique for determining surface structures, and it has already been applied successfully to various QC surfaces.[2] The determination of surface geometries using dynamical LEED requires multiple-scattering calculations to obtain the diffraction intensities from model structures. These intensities are then compared to experimentally measured diffraction intensity spectra. Although the calculation of the multiple scattering is very computer-time-and-space intensive, the development of ever-

faster and bigger computers has allowed LEED analyses for structures having ever larger unit cells. In the case of a QC, however, there is no periodically repeating unit cell, and therefore the number of different atomic environments is infinite. The calculation of the multiple scattering, therefore, requires the use of some rather severe approximations to make the analysis tractable.[3,4]

An earlier LEED analysis of the Al-Ni-Co QC[5] was carried out for a 14-Å-thick slab using the so-called "average transfer matrix approximation (ATA)," which replaces each layer by an atom having the average scattering properties of all atoms in that sublayer. This method is referred to in this paper as method 1. The number of different chemical environments in each sublayer is approximated using the "average neighborhood approximation (ANA)," which replaces

TABLE I. Different atom groups (sublayers) in one QC model layer. Coordination, nearest-neighbor (NN) distance, number of atoms of each type, and the percentage out of all atoms in one layer are given. The coordination of atoms in the outer border and in the center of the slab may differ from these values.

Group name	Coordination	NN distance (Å)	Atoms in one layer	%
TM-1 (Co)	4 or 5	2.43	110	12
TM-2 (Ni)	3	2.43	140	15
Al-1	1	2.24	165	17
Al-2	2	2.43	300	32
Al-3	3	2.43	145	15
Al-4	4 or 5	2.43	85	9

the geometrical environment of each atom with an average environment. In addition, the calculation is further simplified by the "diagonal dominance approximation," where only the diagonal terms in the scattering matrix are retained in the calculation. With these approximations, reasonably good agreement was obtained between the experimental and calculated intensities. However, the nature of the approximations means that much of the geometrical information that one normally seeks in a structure analysis has been lost.

Because of the dominant influence of multiple scattering in LEED, the intensity spectra measured in LEED are strongly influenced by the local structures.[6] The success of the technique called diffuse LEED,[7] which is used to determine local geometries of disordered surfaces by measuring the diffuse scattering in LEED patterns, attests to this. Because these approximations used for QC structures are necessary only to make the multiple scattering calculation tractable, in this paper we propose a different approach. Instead of carrying out an approximate calculation on an "exact" QC structure, we have carried out an exact calculation on an approximate structure. This method is referred to here as method 2. The approximate structure used is periodic instead of a quasiperiodic, but it contains local structures that are expected to be present in the QC structure. Since the structure is well defined, this method allows the positions of in-

dividual atoms to be considered in the analysis. We have applied this approach here to the tenfold surface of decagonal Al-Ni-Co. In this paper, we expand on our previous "method 1"[5] analysis and present new results using the "method 2" approach.

EARLIER WORK ON *d*-Al-Ni-Co STRUCTURES

Decagonal Al-Ni-Co falls into the polygonal class of QC's,[8] with tenfold quasiperiodic order in the plane perpendicular to its periodic direction. Its tenfold symmetry is apparent in the macroscopic QC's, which typically are grown as rods or needles having their axes parallel to the periodic direction, and possess decagon-shaped edges on the cylindrical surface.[9] Decagonal QC's have been studied using many experimental techniques because they have been available as thermodynamically stable, large, high-quality samples for several years. The stable Al-Ni-Co QC structure was discovered by Tsai *et al.* in 1989,[10] and its phase diagram has been extensively studied.[11–13] Al-Ni-Co alloys have at least eight different types of quasicrystalline phases, which exist at various compositions and temperatures.[14] The composition of the sample used in this study, $Al_{73}Ni_{10}Co_{17}$, falls into the basic Co-rich phase. The phase that has the best-characterized bulk structure, however, is the basic Ni-rich structure.

Structural studies of the basic Ni-rich structure suggested that it has a period of about 4 Å along its periodic direction, while the other structures of Al-Ni-Co have diffuse scattering in their x-ray diffraction patterns, which indicate an 8 Å period. The structure of the basic Ni-rich phase has been studied by several different techniques, including electron diffraction and microscopy[15–18] and x-ray diffraction.[19,20] These studies offered several different bulk structure models and prompted several additional models.[18,21–25] Two subsequent x-ray diffraction studies[20,26] were able to rule out some of these proposed models for the bulk structure, including ones that were based on configurations of identical clusters. The conclusion from the high-resolution synchrotron x-ray diffraction study by Cervellino *et al.*[26] was that the only model that is consistent with all of the experimental data consists of recurring structure motifs (clusters) which are not all identical in terms of their atomic arrangements, but which them-

TABLE II. Miller indices, parallel and perpendicular space components of the diffraction vectors, and magnitude of the perpendicular diffraction vector for the beams used in the analysis, The magnitude of the perpendicular diffraction vector is inversely proportional to the spot brightness (energy-averaged) in the diffraction pattern. Beams are sorted with respect to the brightness of the spot, starting with the brightest.

Miller index	$H_{\parallel}x$ (Å^{-1})	$H_{\parallel}y$ (Å^{-1})	$H_{\perp}x$ (Å^{-1})	$H_{\perp}x$ (Å^{-1})	$|H_{\perp}|$
$\overline{1}33\overline{1}$	0	4.32	0	−0.24	0.24
$\overline{1}22\overline{1}$	0	2.67	0	0.39	0.39
$0\overline{1}10$	0	1.65	0	−0.63	0.63
$111\overline{1}$	3.14	0	0.74	0	0.74
$\overline{1}332$	0.97	4.01	−0.60	0.58	0.83
$\overline{1}231$	0.60	3.50	0.97	0.07	0.97
$100\overline{1}$	1.94	0	−1.20	0	1.20

selves have a perfectly quasiperiodic spatial arrangement based on a pentagonal Penrose tiling. Some of the structural details determined in this study rely on certain other measurements, in particular the extended x-ray-absorption fine-structure (EXAFS) study of Zaharko *et al.*, which was able to distinguish between Co and Ni local structures.[27] This structure is consistent with the results of a more recent total-energy based Monte Carlo prediction.[28,29] Interestingly, this x-ray study determined that the periodic spacing is about 8 Å, and not 4 Å, as had been suggested by most other studies for the basic Ni-rich structure, and the ability to make this distinction is attributed to the higher-quality dataset used in this analysis.[26]

The structure proposed by Cervellino *et al.*[26] consists of four different planes of atoms within the 8 Å period. The model consists of two flat layers interspaced with two puckered layers (i.e., flat, puckered, flat, puckered) with the perpendicular (to the plane) displacements of the two puckered layers being opposite in sign.[26] With increasing Co content in this family of QC's, the intensity of the diffuse scattering that indicates the 8 Å period has been observed to increase. Although there have been no similar large dataset x-ray studies carried out on the Co-rich phases, it has been suggested that the increasing diffuse scattering is due to increasing disorder in the stacking of the planes.[20,26]

The tenfold surface structure of Al-Ni-Co has been studied previously using scanning tunneling microscopy (STM), both in the cleaved form[30] and in cut/polished form.[5,31–34]. These studies were carried out on samples having various compositions, but common features were observed in each study. On the cleaved surface, evidence for clusterlike structures was observed, and heat treatments were found to cause only slight changes to the composition of the surface. The STM images of the polished tenfold surface showed a flat, unreconstructed terrace structure, with terraces separated by rough-edged steps of 2.0–2.2 Å height. An earlier spot-profile-analysis low-energy electron diffraction (SPA-LEED) study of this surface had found essentially the same result, i.e., that the step heights correspond to a single atomic step (about 2 Å).[35] Each terrace has local points of fivefold symmetry, which are related by a mirror operation to those in adjacent terraces, consistent with a tenfold screw operation along the periodic axis. The points of fivefold symmetry appear as pentagonal arrangements of protrusions, and the spacing between the pentagons is related by powers of the golden mean τ.[31] A more recent STM study identified two different types of pentagonal features.[33] That study, which also included SPA-LEED and He-atom scattering (HAS) measurements, demonstrated that the structure of the surface is consistent with a truncation of the bulk structure, and that

TABLE III. The momentum vectors, 5D indices, and corresponding approximant indices. Only one each of the symmetry-equivalent 5D vectors and momentum vectors is shown.

Model	Momentum vector (q_x, q_y) (Å^{-1})	5D index	*Approximant indices*
H1	(0 1.65)	(0 −1 −1 0 0)	(2 −2 0), (0 −2 0), (−2 −1 0), (−3 −1 0), (−3 0 0)
	(1.94 0)	(−1 0 0 −1 0)	(3 −2 0), (−1 −2 0), (−3 −1 0), (4 −1 0)
	(0 2.67)	(−1 −2 −2 −1 0)	(3 −3 0), (0 −3 0), (−3 −2 0), (5 −2 0), (−5 0 0)
	(3.14 0)	(1 1 −1 −1 0)	(5 −3 0), (−2 −3 0), (2 −4 0), (−5 −1 0), (6 −1 0)
	(0.60 3.50)	(−1 −2 −3 −1 0)	(5 −4 0), (−1 −4 0), (3 −4 0), (−3 −3 0), (6 −3 0), (−6 −1 0), (7 −1 0), (−7 2 0), (5 2 0)
	(0 4.32)	(−1 −3 −3 −1 0)	(5 −5 0), (0 −5 0), (−5 −3 0), (8 −3 0), (8 −3 0), (−8 0 0)
	(0.97 4.01)	(−1 −3 −3 −2 0)	(6 −4 0), (−2 −4 0), (2 −5 0), (3 −5 0), (−3 −4 0), (7 −4 0), (−7 −1 0), (8 −1 0), (−8 2 0), (6 2 0)
H2	(0 1.65)	(0 −1 −1 0 0)	(−1 −3 0), (3 −2 0), (4 0 0)
	(1.94 0)	(−1 0 0 −1 0)	(−3 −3 0), (0 −4 0), (4 −1 0)
	(0 2.67)	(−1 −2 −2 −1 0)	(−2 −5 0), (5 −3 0), (6 0 0)
	(3.14 0)	(1 1 −1 −1 0)	(−4 −5 0), (0 −6 0), (7 −2 0)
	(0.60 3.50)	(−1 −2 −3 −1 0)	(−4 −6 0), (1 −7 0), (6 −5 0), (8 −1 0), (7 3 0)
	(0 4.32)	(−1 −3 −3 −1 0)	(−3 −8 0), (8 −5 0), (10 0 0)
	(0.97 4.01)	(−1 −3 −3 −2 0)	(−5 −7 0), (1 −8 0), (6 −6 0), (9 −2 0), (9 3 0)
B1	(0 1.65)	(0 −1 −1 0 0)	(2 −3 0), (3 −2 0), (3 0 0), (0 −3 0), (2 2 0)
	(1.94 0)	(−1 0 0 −1 0)	(1 −4 0), (4 −1 0), (3 −3 0), (3 1 0), (−1 −3 0)
	(0 2.67)	(−1 −2 −2 −1 0)	(3 −5 0), (5 −3 0), (5 0 0), (0 −5 0), (3 3 0)
	(3.14 0)	(1 1 −1 −1 0)	(2 −6 0), (6 −2 0), (5 −5 0), (5 2 0), (−2 −5 0)
	(0.60 3.50)	(−1 −2 −3 −1 0)	(3 −7 0), (7 −3 0), (6 −5 0), (5 −6 0), (7 −1 0), (1 −7 0), (5 3 0), (−3 −5 0), (1 −6 0), (−6 1 0)
	(0 4.32)	(−1 −3 −3 −1 0)	(5 −8 0), (8 −5 −0), (8 0 0), (0 −8 0), (5 5 0)
	(0.97 4.01)	(−1 −3 −3 −2 0)	(3 −8 0), (8 −3 0), (7 −6 0), (6 −7 0), (8 2 0), (2 −8 0), (6 3 0), (−3 −6 0), (2 7 0), (−7 −2 0)

its structure can be identified with a random (as opposed to ideal) quasicrystalline tiling.

This was also the conclusion of a different STM study.[34] In that study, ion scattering spectroscopy (ISS) and Auger electron spectroscopy (AES) were employed to determine the surface composition, which was found to be Al-rich and having an average atomic density about 35% lower than a bulk-truncated plane.

EXPERIMENT

The QC used in this study was grown at Ames Laboratory by a slow cooling technique, as described previously.[36] Resulting quasicrystals, up to several mm in length and diameter, were separated from the remaining melt by decanting in a centrifuge. The composition of this sample, measured by electron microprobe analysis, is $Al_{73}Ni_{10}Co_{17}$. According to the phase diagram for Al-Ni-Co,[14] this composition falls into the region of the basic Co-rich phase. The resulting rod, about 5 mm in diameter with its axis parallel to the periodic direction, was cut to a thickness of about 2 mm and polished on both sides using a diamond abrasive. The final polish was done using 0.25 μm size grit, and the resulting surfaces had the appearance of mirrors. Laue diffraction was used to verify that the surface was within 0.5° of the tenfold orientation.

The sample preparation in ultrahigh vacuum consisted of Ar ion bombardment (500 eV ions) for about 30 min, followed by annealing for 6–8 h at temperatures up to 1060 K, as measured by a K-type thermocouple and an optical pyrometer [using emissivity=0.35 (Ref. 32)]. The quality of the surface, as judged by the quality of the LEED pattern, was observed to improve with extended annealing. After preparation, the LEED pattern was observed to have well-defined spots and relatively low diffuse scattering, as shown in Fig. 1. The symmetry of the LEED pattern is tenfold, due to the presence of two equivalent surface terminations rotated by
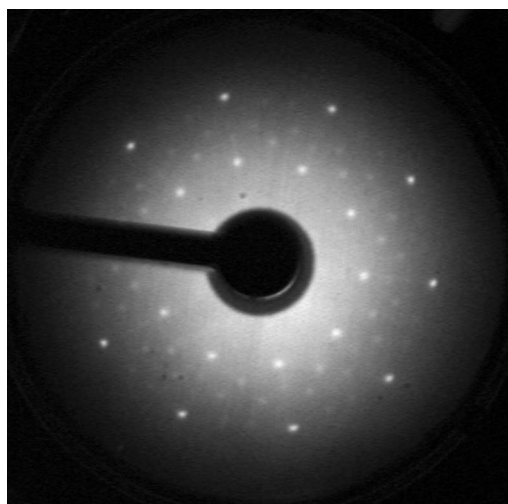

FIG. 1. LEED pattern from Al-Ni-Co for a primary beam energy of 68 eV and sample T=60 K.

36°.[2] The impurity level was below detectablility, measured by AES, as shown in Fig. 2.

AES was used to monitor the composition of the surface during the *in situ* preparation process, to compare it with the bulk composition of $Al_{73}Ni_{10}Co_{17}$. With the assumption of uniformity of the composition of the surface plane, we used a standard method to derive the chemical composition of the surface from the AES data;[37,38] because of the intrinsic difficulty in discriminating the Ni and Co peaks (which overlap in the energy range of 600–800 eV), we considered those elements only as transition metals. After a typical cycle of sputtering, the chemical composition of the surface derived with this method was $Al_{63}TM_{37}$. The same surface after a cycle of annealing at T=1060 K had a chemical composition of $Al_{71}TM_{29}$. A similar increase of Al concentration after annealing was observed using ISS from a similar AlNiCo surface,[34] although in that case, the composition after anneal-

TABLE IV. Perpendicular coordinates (z) for each atom in the top four layers of the H1 approximant. The positive direction is toward the bulk. The numbers associated with the atomic labels in the first layer represent the atoms as shown in Fig. 4(a). TM-1=Co; TM-2=Ni.

| Layer 1			Layer 2		Layer 3		Layer 4	
z (Å)	Identity		z (Å)	Identity	z (Å)	Identity	z (Å)	Identity
0.00±0.08	Al-3	1	2.00±0.12	Al-2	4.2±0.2	Al-1	6.37	Al
0.00±0.08	Al-3	1	2.00±0.12	Al-2	4.23±0.10	Al-2	6.37	Al
0.04±0.11	Al-1	2	2.1±0.2	Al-2	4.23±0.10	Al-2	6.37	Al
0.12±0.04	TM-1	3	2.1±0.2	Al-2	4.26±0.12	Al-4	6.37	Al
0.14±0.04	TM-2	4	2.11±0.06	TM-2	4.26±0.10	TM-2	6.37	Al
0.15±0.09	Al-2	5	2.11±0.06	TM-2	4.27±0.08	TM-1	6.37	Al
0.15±0.09	Al-2	5	2.2±0.2	Al-3	4.27±0.11	Al-2	6.37	Al
0.16±0.06	Al-2	6	2.2±0.2	Al-3	4.27±0.11	Al-2	6.37	Al
0.16±0.06	Al-2	6	2.24±0.07	TM-2	4.3±0.2	Al-2	6.37	TM-1
0.26±0.10	Al-4	7	2.26±0.06	TM-1	4.32±0.11	Al-3	6.37	TM-2
0.28±0.04	TM-2	8	2.3±0.2	Al-4	4.32±0.11	Al-3	6.37	TM-2
0.28±0.04	TM-2	8	2.4±0.2	Al-2	4.34±0.05	TM-2	6.37	TM-2
0.32±0.13	Al-2	9			4.34±0.05	TM-2		
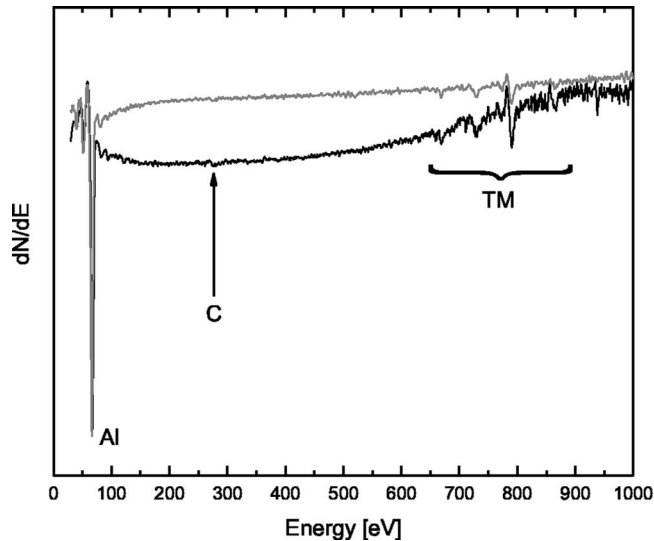
FIG. 2. Auger spectra from Al-Ni-Co after different stages of the preparation procedure: after sputtering (black curve) and after annealing (gray curve). At this preparation stage, there is still a small amount of residual C.

ing was found to be $Al_{89}TM_{11}$. In that same study, AES, which probes the top several layers as opposed to just the top layer in ISS, was found to give a composition closer to that of the bulk,[34] consistent with the measurements presented in Fig. 2.

The LEED intensities were measured using a rear-view LEED system, with the electron beam at normal incidence to the surface. The sample temperature was held at 60 K, as measured by the thermocouple, to minimize thermal effects. The data were acquired using a monochromatic CCD camera interfaced to a personal computer via a Data Translation frame grabber board. Data were acquired in steps of 1 eV, and for each energy step, 20 images were acquired and averaged to reduce electronic noise, and stored for later analysis. The $I(E)$ curves were extracted by integrating the spot intensity in circular windows centered on the diffraction spots. The background intensity for each spot was determined by fitting a planar background to the perimeter of the integration window. The background was then subtracted from the integrated intensity. The intensity curves from symmetry-equivalent spots were averaged to improve the statistics. Finally, the $I(E)$ curves were smoothed using a three-point smooth.

LEED COMPUTATIONS

Method 1: QC structure model

The initial coordinates used for the atoms of one QC layer in this study are those determined by the x-ray diffraction study of Steurer *et al.*[19] for $Al_{70}Ni_{15}Co_{15}$. The top view of one layer of atoms is shown in Fig. 3. The separation between the transition metals (TM) and aluminum atoms is also

TABLE V. Perpendicular coordinates (z) for each of the atoms in the top three layers of the approximant B1. The positive direction is toward the bulk. The numbers associated with the atomic labels in the first layer represent the atoms as shown in Fig. 4(c). TM-1=Co; TM-2=Ni.

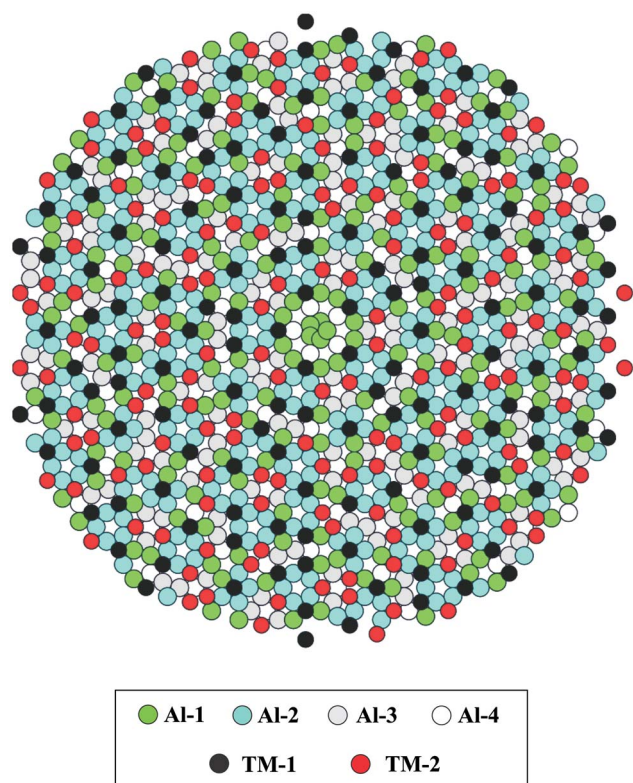| Layer 1			Layer 2		Layer 3	
z (Å)	Identity		z (Å)	Identity	z (Å)	Identity
0.0±0.2	Al-4	1	1.8±0.3	Al-3	4.10	Al
0.00±0.12	Al-1	2	1.8±0.3	Al-3	4.10	Al
0.00±0.12	Al-1	2	1.9±0.2	Al-2	4.10	Al
0.00±0.03	TM-2	3	1.9±0.2	Al-2	4.10	Al
0.00±0.03	TM-2	3	1.9±0.2	Al-1	4.10	Al
0.00±0.14	Al-2	4	1.9±0.2	Al-1	4.10	Al
0.00±0.14	Al-2	4	2.0±0.3	Al-4	4.10	Al
0.01±0.06	TM-1	5	1.98±0.09	TM-2	4.10	Al
0.05±0.12	Al-3	6	1.98±0.09	TM-2	4.10	Al
0.05±0.12	Al-3	6	2.0±0.3	Al-1	4.10	Al
0.08±0.12	Al-1	7	2.09±0.06	TM-1	4.10	Al
0.08±0.12	Al-1	7	2.09±0.06	TM-1	4.10	Al
0.15±0.08	Al-4	8	2.10±0.13	TM-1	4.10	Al
0.15±0.08	Al-4	8	2.2±0.3	Al-2	4.10	Al
0.16±0.12	Al-2	9	2.2±0.3	Al-2	4.10	Al
0.16±0.12	Al-2	9	2.19±0.12	TM-2	4.10	Al
0.19±0.04	TM-2	10	2.19±0.12	TM-2	4.10	TM-1
0.19±0.04	TM-2	10	2.2±0.3	Al-3	4.10	TM-2
0.2±0.2	Al-3	11	2.2±0.3	Al-3	4.10	TM-2
0.2±0.2	Al-3	11			4.10	TM-2
0.3±0.3	Al-1	12			4.10	TM-2

FIG. 3. (Color online) Top view of the fivefold QC layer. The different atomic groups are described in Table I.

based on the same study. This structure model is very similar to that determined by the later study for $Al_{70}Ni_{23}Co_7$,[26] except that it does not explicitly include fractional occupancy of the atom sites, and the buckling of the layers was not included. Because it is difficult to distinguish between Co and Ni atoms by x-ray or electron diffraction, no distinction of TM atoms into Ni and Co was made in the initial dataset. Most of the atoms in the coordinate set thus reside on the vertices of a rhombic Penrose tiling with edge length 2.43 Å, which is related to the pentagonal Penrose tiling by an inflation symmetry operation.[26]

Although the phase studied in this paper, the basic Co-rich structure, is not the same as those studied in the x-ray diffraction studies, the diffraction pattern is similar, and accord-

TABLE VI. Average interlayer spacings dz and intralayer bucklings Δ for the best-fit structure for all models. The best Pendry R-factor for each model is given on the last line.

Parameter	H1 (Å)	H2 (Å)	B1 (Å)	QC (Å)
dz_{12} (average)	2.01±0.09	2.0±0.2	1.9±0.2	1.84±0.13
dz_{23} (average)	2.1±0.1		2.1±0.2	2.14±0.14
dz_{34} (average)	2.1±0.1			2.0±0.2
dz_{bulk}	2.04	2.04	2.03	2.04
Δ_1 (average)	0.08±0.06	0.1±0.2	0.07±0.1	0.06±0.1
Δ_2 (average)	0.1±0.1			0.08±0.1
Δ_3 (average)	0.04±0.1			0.03±0.1
R_P	*0.26*	*0.36*	*0.26*	*0.32*

ing to Ritsch *et al.*,[14] only a few weak additional reflections are observed in the basic Co-rich phase compared to the basic Ni-rich phase. The Co-rich phase is thought to exhibit more disorder and random tiling compared to the perfect tiling of the basic Ni-rich phase. In our study, no additional spots in the diffraction pattern were observed.

In this calculation, the atoms in each QC layer are separated into six different groups (sub-layers). The atoms that belong to each group are treated as if they have the same scattering properties parallel to the surface (ANA). The transition metals are separated into two groups depending on the types of their nearest neighbors (NN). In the EXAFS study,[27] different local environments for transition-metal atoms in the *d*-Al-Ni-Co QC were proposed. For Ni, the NN distribution is found to be bimodal, i.e., there are two characteristic NN distances, suggesting that both Al and TM atoms are present. For Co, the distribution appears to have just one NN distance corresponding to Al atoms. In this calculation, group TM-1 has only Al as NN, and atoms in group TM-2 have a bimodal NN distribution, with the nearest neighbors being either Al or Ni. This separation is somewhat artificial since LEED is not very sensitive to the difference between Ni and Co atoms, but the separation allows for the possibility of buckling between the two groups of TM metals.

The separation between different groups of aluminum atoms has been done using simply the number of nearest neighbors (whether they are Al or TM). Group Al-1 corresponds to atoms that are coordinated to one atom. This atom pairs with its equivalent atom in the layer below or above it. The NN distance is short, 2.24 Å, which indicates that the occupancy of these sites cannot be 1.00. In these calculations, the occupancy of atoms of this type is fixed at 0.50. Al-2 and Al-3 atoms have coordinations of 2 and 3, respectively, and together with the TM-2 atoms, form the 10-rings that consist of pentagons that are rotated by 36° in alternating layers. These 10-rings form decaprismatic columnar clusters.[19] The center of a pentagon in a columnar cluster can be either empty or filled. The last group of Al atoms, Al-4, is the group of atoms that reside in the center of these pentagons, and thus have coordination 4 or 5. The centers of the pentagons can be occupied only in every other layer; otherwise there would be unreasonably short (2.04 Å) NN distances.

Since most of the atoms in the coordinate set reside in the vertices of the rhombic Penrose tiling with an edge length of 2.43 Å, the dominant NN distance is 2.43 Å. This is, in general, too short for an Al-Al bond, but is more reasonable for an Al-TM bond (atomic radii in bulk for Ni, Co, and Al are 1.43, 1.25, and 1.25 Å, respectively). To reduce the number of unfavorable Al-Al bonds, the occupancy of all atoms is set to 0.90 (apart from the atoms in the Al-1 group, which have an occupancy of 0.50) at the beginning of the analysis. The method of using partial occupancies was exploited in the x-ray diffraction study of the basic Ni-rich phase as a means of preventing unphysical NN distances, of creating structures that have realistic densities, and also of introducing disorder into the structure.[26] The different atom groups are summarized in Table I. The QC slab used in the calculation is built by stacking the layers described above in an *ABAB* sequence, where the layers *A* and *B* are related by a 36° rotation. Indi-

vidual layers have fivefold symmetry, but by virtue of this stacking sequence, the unrelaxed slab possesses a tenfold screw axis. In these calculations, a slab thickness of about 14 Å (eight layers) and a radius of about 50 Å was used.

The interlayer distance of the bulk structure, 2.04 Å,[19,26] was used as a starting point in this calculation. The 8 Å period discussed before is not necessarily relevant to the surface layers and was not explicitly included here. However, its presence (or not) can manifest itself in the variable interlayer spacing and the buckling of the layers. The separation of the different atom types, discussed in the previous section, was done in the top four layers. In the bottom two layers, the fraction of Ni and Co atoms, relative to the total number of TM atoms, was set to 0.4 and 0.6, respectively. This gives a corresponding composition of $Al_{74}Ni_{11}Co_{15}$ for these two layers, compared to the measured bulk composition of $Al_{73}Ni_{10}Co_{17}$. Intralayer buckling was allowed between the different atom types (sublayers) in the four top layers and the two bottom layers were constrained to be planar. This kind of separation produces 26 free geometrical parameters, which gives a data length of 68 eV per parameter.

The LEED calculations for the QC model were carried out using the LEED program of Moritz[39] that had been modified for quasicrystalline stuctures,[4] including the ATA and ANA approximations. The agreement was tested using the Pendry R-factor.[40]

Method 2: Periodic approximant structure models

Periodic approximants for quasicrystalline d-AlNiCo are constructed by imposing a linear phason strain to the atomic surfaces of the five-dimensional (5D) hypercubic lattice.[41] Periodic structures for many different alloys, including d-Al-Ni-Co, are given at the alloy database website http://alloy.phys.cmu.edu/. The unit cell size for the various d-Al-Ni-Co approximants range from 25 to 214 atoms per unit cell. The choice of approximant used in the quantitative LEED calculation is limited by both the computer power available and by the size of the experimental data set.

In this analysis, three different approximants were used, shown in Fig. 4. The H1 and H2 approximants represent similar local structures, but H2 has a unit cell that has twice as many atoms as H1. Both models are based on local structures that are dominated by pentagons of transition-metal atoms. The third approximant used, B1, represents a different local structure, which consists of overlapping decagons of transition-metal atoms.

The H1 approximant structure [Fig. 4(a)] has 25 atoms per unit cell, in two periodically repeating layers of 13 and 12 atoms, respectively. The composition of this structure is $Al_{68}Ni_{24}Co_8$. There is a mirror plane in the unit cell. The H2 approximant structure [Fig. 4(b)] has 50 atoms per unit cell, in two repeating layers having 26 and 24 atoms per layer. This unit cell has no reflection symmetry, but its composition is also $Al_{68}Ni_{24}Co_8$. Figure 4(c) shows the B1 approximant structure, which has 40 atoms per unit cell, divided into two layers of 21 and 19 atoms, respectively. There is a mirror plane in this unit cell, which has the composition $Al_{72.5}Ni_{20}Co_{7.5}$. Because LEED cannot distinguish between
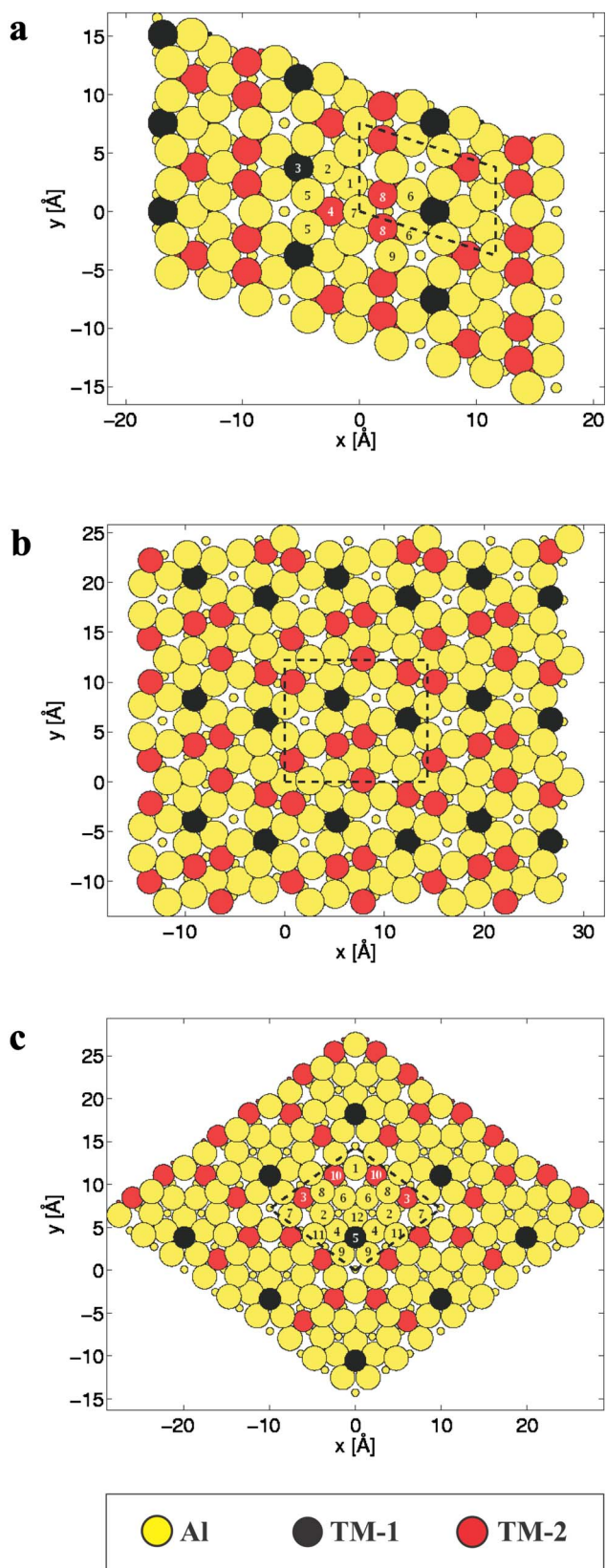

FIG. 4. (Color online) Top view of the model structures of the approximants a) H1, b) H2, c) B1. The dashed lines show the unit cell. The larger circles correspond to atoms in the top layer, and the smaller circles to atoms in the second layer. The numbers are used to identify atoms in Tables IV and V.

Co and Ni, the compositions of the approximants can be considered to be $Al_{68}TM_{32}$ for H1 and H2, and $Al_{72.5}TM_{27.5}$ for B1.

Since we are using periodic structures to approximate quasiperiodic structures, we need to match the diffraction beams of the two types of structures. The beam indexing was done in the following way. Five basis vectors are needed to generate the reciprocal lattice of a decagonal QC. The diffraction vector $\mathbf{H}_{\parallel}$ can be calculated from

$$\mathbf{H}_{\parallel} = \sum_{j=1}^{5} h_j \mathbf{b}_j, \tag{1}$$

where h_j are Miller indices and

$$\mathbf{b}_j = b\left(\sin\left(\frac{2\pi j}{5}\right), \cos\left(\frac{2\pi j}{5}\right), 0\right), \quad j = 1, \ldots, 4 \tag{2}$$

and

$$\mathbf{b}_5 = b_5(0,0,1), \tag{3}$$

where $b = 1.02$ Å^{-1} and $b_5 = 0.78$ Å^{-1}.[42] Four of these basis vectors point to the corners of a regular pentagon (the fifth corner of the pentagon is a linear combination of the other four) and the fifth basis vector is perpendicular to the surface (i.e., parallel to the tenfold axis). The Miller indices of the four independent unit vectors parallel to the surface are (10000), (01000), (00100), and (00010). The unit vector perpendicular to the surface is (00001). The indexing scheme is shown graphically in Fig. 5. Seven different diffraction beams were used in this analysis. These beams can be identified by four Miller indices because the fifth vector is pointing into the surface. The indices of the beams used in the calculation are $(0\bar{1}\bar{1}0)$, $(\bar{1}2\bar{2}1)$, $(1\bar{1}\bar{1}\bar{1})$, $(\bar{1}3\bar{3}1)$, $(\bar{1}3\bar{3}2)$, $(100\bar{1})$, and $(\bar{1}2\bar{3}1)$. The corresponding diffraction vectors $\mathbf{H}_{\parallel}$ calculated using Eq. (1) are (0, 1.65), (0, 2.67), (3.14, 0), (0, 4.32), (0.97, 4.01), (1.94, 0), and (0.60, 3.50).

Decagonal QC's can be embedded in a five-dimensional superspace, and this embedding and the decomposition are discussed elsewhere in detail.[26,43–45] Briefly, the basis vectors $\mathbf{b}_j$ $(j=1,\ldots,5)$ are the physical space (parallel space) projection of the 5D reciprocal space vectors. This 5D space can be divided into parallel (3D) and perpendicular (2D) spaces.
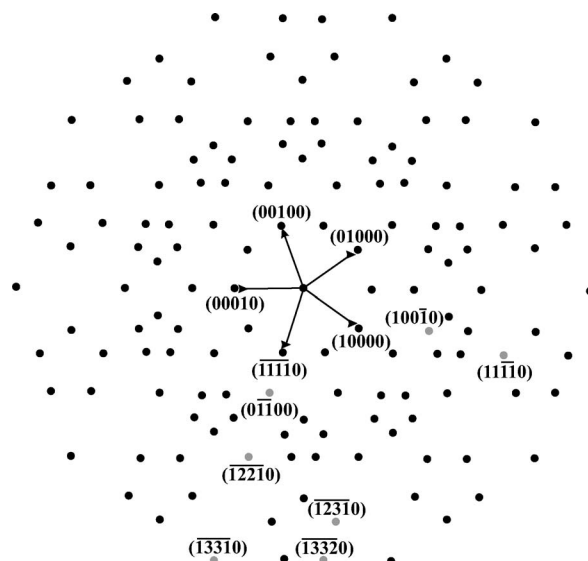

FIG. 5. Schematic diagram of the diffraction pattern showing the beam index scheme used in this study. The central spot is the (00000) beam. The spots in light gray shading correspond to the experimental beams considered in the analysis.

The parallel ("physical") space has diffraction vectors $\mathbf{H}_{\parallel}$ given by Eq. (1), and the perpendicular space basis vectors $\mathbf{b}'_j$ can be written as

$$\mathbf{b}'_j = b\left(\sin\left(\frac{6\pi j}{5}\right), \cos\left(\frac{6\pi j}{5}\right)\right), \quad j = 1, \ldots, 4. \tag{4}$$

Diffraction vectors associated with $\mathbf{b}'_j$ ($\mathbf{H}_{\perp}$) can be calculated from

$$\mathbf{H}_{\perp} = \sum_{j=1}^{4} h_j \mathbf{b}'_j. \tag{5}$$

The magnitude of the diffraction vector in perpendicular space is associated with the brightness of the beam: the larger $|\mathbf{H}_{\perp}|$ is, the weaker is the intensity of the diffraction spot. Table II shows the Miller indices and the parallel and perpendicular space vectors for the beams used in this analysis.

The approximant beam indices are generated by expressing the pseudopentagonal basis of the QC in the reciprocal space of the approximant. Then all symmetry-related 5D in-

TABLE VII. The components of each atom type for each model considered here. Al-1 atom sites are only half occupied in the QC model. In the H1 approximant, Al-1 atoms appear in every other layer. In the H2 approximant, the number of Al-1 atoms alternates between four and two in adjacent layers. In the B1 approximant, the number of Al-1 atoms alternates between five and three in adjacent layers.

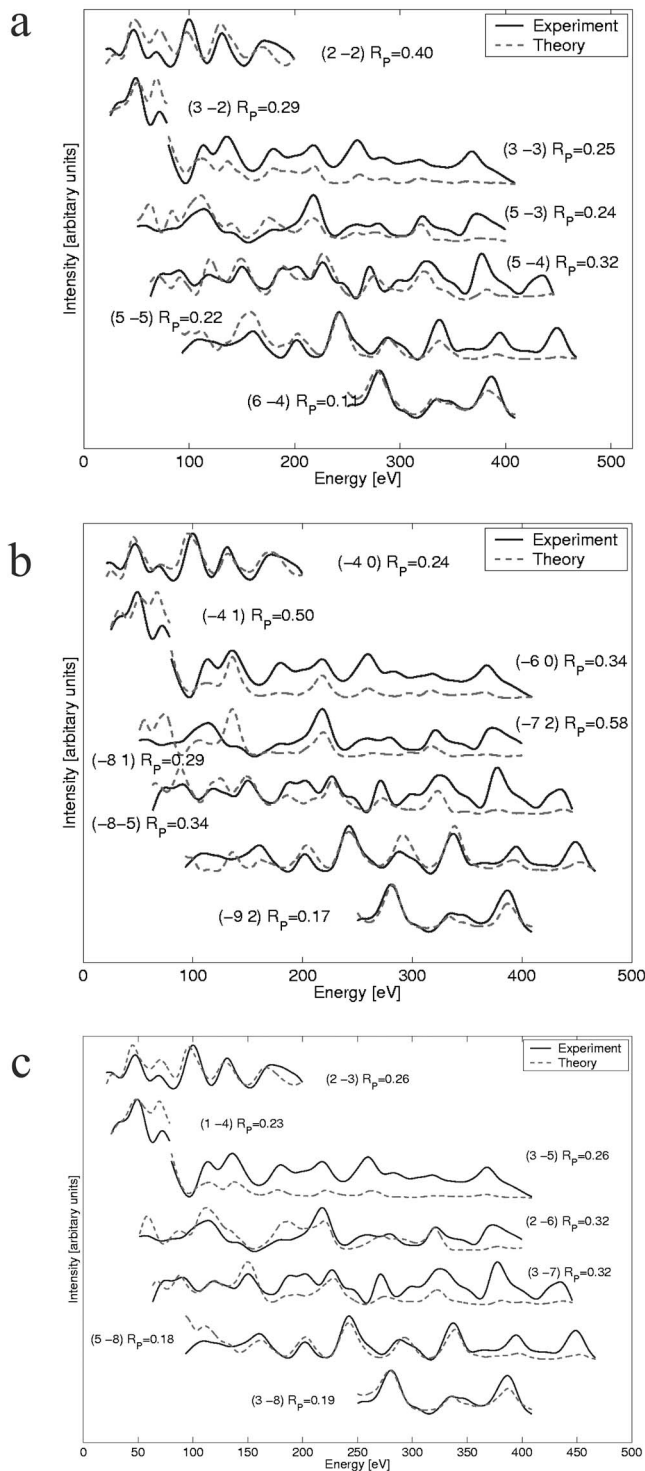|		QC model	H1	H2	H3
Aluminum	Al-1	17%	4%	12%	20%
	Al-2	32%	40%	32%	20%
	Al-3	15%	16%	16%	20%
	Al-4	9%	8%	8%	10%
Cobalt	TM-1	12%	8%	8%	10%
Nickel	TM-2	15%	24%	24%	20%

FIG. 6. $I(E)$ curves for the favored structure using the (a) H1, (b) H2, and (c) B1 approximant models, along with the Pendry R-factors for each beam. The solid curves are the experiment, and the dashed ones are the calculation. The overall Pendry R-factor is 0.26 for H1, 0.36 for H2, 0.26 for B1.

dices for a given $Q=\sqrt{q_1^2+q_2^2}$ are expressed in terms of the pseudopentagonal basis. For each Q, there are ten symmetry-related 5D indices. Each approximant index corresponds to one of these 5D indices. However, not all 5D indices have their counterpart in the approximant's reciprocal space. To retain the symmetry of the diffraction pattern (tenfold), the approximant indices for each Q are averaged together with equal weights. Table III shows the approximant indices for H1, H2, and B1, corresponding to the 5D indices used in our earlier analysis.[5]

The LEED calculations were performed using the Barbieri/Van Hove Symmetrized Automated Tensor LEED package.[46,47] The theory-experiment agreement was tested using the Pendry R-factor[40] and error bars were calculated using the Pendry RR-function.[40] Crystal potentials for Al, Ni, and Co were characterized using phase shifts up to $l_{max}=8$ obtained from the Barbieri/Van Hove Phase Shift Package.[47] The other nonstructural parameters include the bulk Debye temperatures for Al (428 K), Ni (450 K), and Co (445 K) and the imaginary part of the inner potential ($V_i=-5$ eV). The real part of the inner potential was assumed to be energy-independent and was allowed to vary to obtain optimal agreement. The bulk Debye temperatures were used for the surface layers and were not optimized. The energy range for the theoretical calculation was 20–470 eV, and the total range of the experimental data was 1835 eV.

RESULTS AND DISCUSSION

In the structural analyses for all models, only the relaxations of different atom groups perpendicular to the surface were considered. This means that interlayer relaxations and intralayer buckling were allowed, but lateral shifts of atoms are not. The results of the QC analysis have been presented before.[5] To recap briefly, the average interlayer spacings were found to be $d_{12}=1.84$ Å, $d_{23}=2.14$ Å, $d_{34}=2.0$ Å, $d_{45}=2.1$ Å, and $d_{56}=2.0$ Å. The magnitudes of the buckling in the top four layers were 0.06 ± 0.10 Å, 0.08 ± 0.14 Å, 0.03 ± 0.14 Å, and 0.1 ± 0.2 Å, respectively. The best Pendry R-factor was 0.32.

For the H1 approximant, two different terminated structures were considered, one with a 12-atom top layer and one a 13-atom top layer. The level of agreement was similar for the two terminations, being slightly better for the 13-atom termination. The optimization allowed the z coordinates of each of the top three layers to vary. Because of the symmetry, this optimization results in 27 free parameters, giving 68 eV per parameter. The optimum structure has a contracted first interlayer spacing and an expanded second and third interlayer spacings. There is some buckling in the first two layers, but the third layer is almost flat. Table IV gives the geometrical parameters for the atoms in the favored structure. The best R_P obtained was 0.26. Figure 6(a) shows the experimental and calculated intensity spectra for H1.

For the H2 approximant, the two possible terminations have 24 and 26 atoms, respectively. Again the denser layer was slightly preferred for the termination. The optimization included the z coordinates for the top-layer atoms. This gives 26 free parameters or 71 eV per parameter. The lack of symmetry in the unit cell effectively prevented including relaxations of the deeper layers in this analysis due to the large number of parameters it would involve. R_P for the favored structure was 0.36. Figure 6(b) shows the intensity spectra.
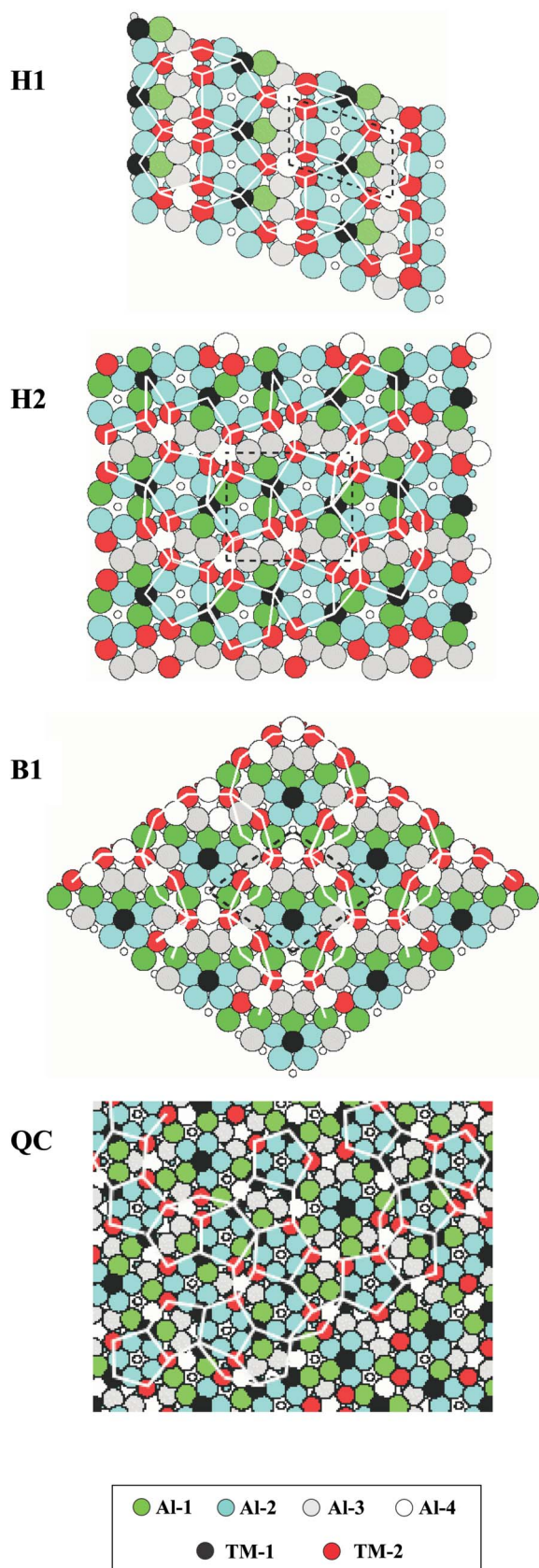
FIG. 7. (Color online) Tilings for the different structure models used. The larger circles correspond to atoms in the top layer, and the smaller circles to atoms in the second layer.

The H2 model has similar features and similar results to the H1 model, but worse agreement because the positions of atoms below the top layer cannot be adjusted in the analysis.

For the B1 approximant, the level of agreement was essentially identical for the two termination layers having 19 and 21 atoms, respectively. The surface with 19 atoms has more TM atoms (4 Ni+3 Co) than the surface that terminates with 21 atoms (4 Ni+1 Co). Both terminations were considered in the optimization, which included the z coordinates of the top two layers of atoms in both cases. This gives 24 free parameters, or 76 eV/parameter. The 21-atom termination was favored over the 19-atom termination, giving optimized R_P of 0.26 and 0.31, respectively. The first interlayer spacing is slightly contracted and the second interlayer spacing is somewhat expanded, relative to the bulk. The geometrical parameters are given in Table V, and Fig. 6(c) shows the intensity spectra.

Table VI presents a summary of the main features of the structures obtained with the four different structure models. The results of all analyses are similar. Each structure has some degree of contraction of the first interlayer spacing, and for the analyses where it was included, some expansion of the second interlayer spacing. The degree of contraction found was smaller for the approximant models than for the QC model. The degree of intralayer buckling found using the different models was quite similar. The distinction between Co and Ni can be considered as artificial. The ability to distinguish between them was tested in the LEED analysis using the H1 structure and it was found that the TM atoms can be assigned arbitrarily to Co and Ni without a change in the result.

The ability to relax the atoms individually in the H1 and B1 analyses provides insight into whether good choices were made for the "separations" into sublayers using the method 1 analysis. To assess this, a criterion is needed to identify the atoms in the QC model with those in the approximant models. To this end, tilings were used to identify which atoms were similar (according to their neighborhood) in the different models. The starting point was to draw a tiling of pentagons and rhombi on the H1 approximant, placing the vertices at the locations of transition-metal atoms. The H2 approximant has the same tiling structure as the H1—for both H1 and H2, the surface can be completely filled with a tiling having pentagons and rhombuses, shown in Fig. 7. When the QC model is tiled in a similar way, the parts of the surface that are left over (not included in the tiled area) are shaped like decagons. The B1 approximant, which was chosen in order to represent parts of the real surface that are not represented in the H1/H2 tilings, can be tiled entirely with overlapping decagons, also shown in Fig. 7. Almost all of the atoms forming the QC structure can be assigned to one of these two tilings. Using this connection between the local structures of the QC model and the approximant models, a new separation scheme can be devised.

In Fig. 7, the atom identification scheme from the QC model of Fig. 3 has been transferred to the approximant models by using the two tilings as a guide. With this scheme, the H1 and H2 structures are dominated by pentagons of Al-2 atoms. The B1 approximant is dominated by "flowers," which have one TM-1 (Co) atom at their centers surrounded

TABLE VIII. Atomic positions of different atomic groups with respect to the center of mass of the layer, for each model. In the first column on the left, the center-of-mass position of each layer is given in parentheses. The positive direction is toward the bulk and units are Å. For the approximant models, multiple values are listed for one layer, since there can be several different inequivalent atoms in one group.

	Al				Co	Ni
	Al-2	Al-3	Al-4	Al-1	TM-1	TM-2
QC model						
1st (0.00 Å)	−0.08±0.06	0.0±0.2	0.01±0.06	0.1±0.2	−0.08±0.03	0.06±0.06
2nd (1.84 Å)	−0.08±0.07	0.1±0.2	0.1±0.2	−0.2±0.3	0.03±0.06	0.07±0.07
3rd (3.98 Å)	0.00±0.06	−0.1±0.3	0.03±0.09	0.0±0.3	−0.01±0.05	0.02±0.07
H1 model						
1st (0.00 Å)	−0.01±0.09	−0.16±0.08	0.10±0.10	−0.12±0.11	−0.04±0.04	−0.02±0.04
	0.00±0.06					0.12±0.04
	0.16±0.13					
2nd (2.01 Å)	−0.17±0.12	0.1±0.2	0.2±0.2		0.09±0.06	−0.06±0.06
	−0.1±0.2					0.07±0.07
	0.2±0.2					
3rd (4.12 Å)	−0.05±0.10	0.04±0.11	−0.02±0.12	−0.1±0.2	−0.01±0.08	−0.02±0.10
	−0.01±0.11					0.06±0.05
	0.0±0.2					
B1 model						
1st (0.00 Å)	−0.09±0.14	−0.04±0.12	−0.1±0.2	−0.09±0.12	−0.08±0.06	−0.09±0.03
	0.07±0.12	0.1±0.2	0.06±0.08	−0.01±0.12		0.10±0.04
				0.2±0.3		
2nd (1.93 Å)	−0.2±0.2	−0.2±0.3	−0.1±0.3	−0.1±0.2	0.07±0.06	−0.04±0.09
	0.1±0.3	0.2±0.3		0.0±0.4	0.08±0.13	0.17±0.12

by four Al-2 and one Al-1 atoms. These "pentagons" and "flowers" can also be identified in the QC model. Table VII gives the percentages of each atom group in each model. Using this identification, Table VIII gives the positions of each atom group for each model, with respect to the center of mass of the layer. One should not compare the details of the H and B models with each other since they correspond to different local structures. It is more relevant to compare the approximant models with the QC model.

The identification of groups of atoms that correspond to similar geometric patterns in the approximant models, and the comparison of these groups with the QC model, suggest a different separation scheme using those groups, as shown in Fig. 8. In this scheme, TM atoms are separated into two groups (nominally identified as Ni and Co). Al atoms are separated into three different groups: Al-A consists of pentagonal clusters of Al atoms surrounded by five TM atoms; Al-B consists of triangular clusters of Al atoms, surrounded by five TM atoms; Al-C includes all the remaining Al atoms. The pentagonal tiles corresponding to the Al-A and Al-B clusters can be identitied in the QC slab. The resulting tiling is isomorphic to a Penrose tiling, as shown in Fig. 8. The QC model analysis was repeated using this new separation into the five different groups, using the separations given above for the five layers. This gives 25 adjustable parameters, compared to 26 used in the first QC analysis. The agreement between the experimental and calculated spectra improved significantly even though the number of optimized

TABLE IX. Atomic positions of different atom groups with respect to the center of mass of each layer. The locations of the centers of mass for each layer are given in the first column in parentheses. The negative direction is toward the vacuum. The atomic groups are shown in Figs. 8 and 9.

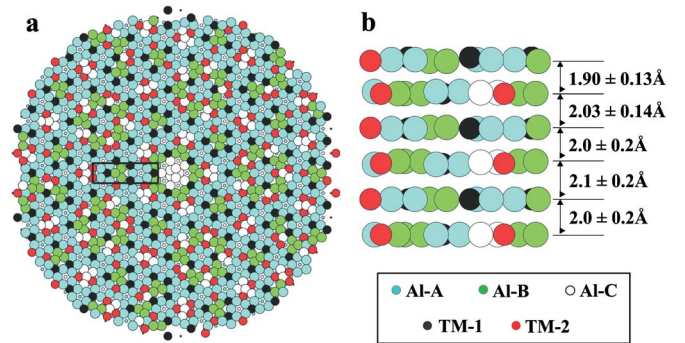| QC model 2 (Fig. 9)	Al (Å)			Co (Å) TM-1	Ni (Å) TM-2
	Al-A	Al-B	Al-C		
1st layer (0.00 Å)	−0.03±0.03	0.1±0.3	0.1±0.2	−0.16±0.03	0.04±0.05
2nd layer (1.90 Å)	−0.08±0.07	0.0±0.03	0.0±0.2	0.03±0.06	0.04±0.07
3rd layer (3.93 Å)	0.03±0.06	0.0±0.3	0.0±0.3	0.02±0.05	−0.02±0.07
4th layer (5.95 Å)	0.07±0.12	−0.1±0.3	−0.1±0.2	0.04±0.06	0.02±0.10
5th layer (8.02 Å)	0.00±0.12	0.0±0.3	0.0±0.2	0.00±0.08	0.00±0.12

FIG. 9. (Color online) Optimized final structure. (a) Top view; (b) side view [viewing black box in (a) from the bottom]. The interlayer spacings are exaggerated for clarity.

with perfect tilings, and no attempt has been made to introduce a random tiling effect. We have not yet integrated the possibility of random tiling into this type of analysis, but this is something that could be explored in future studies.

CONCLUSION

This paper has presented a new method for analyzing the LEED intensity data from quasicrystal surfaces. The method consists of using periodic approximant structures as structure models instead of a slab having a long-range quasicrystal structure. This allows one to use existing LEED programs without modification, and without the severe approximations that are required for the QC slab model. The only significant approximation used in the approximant analysis is the structure model itself, as an approximation to the quasicrystal. By using periodic approximant structures with limited numbers of atoms in each unit cell, it is possible to allow the positions of every atom in the structure to be adjusted. The factors which limit the useful size of the approximant unit cell are the length of the experimental dataset and the amount of symmetry present in the unit cell. In the cases described here,

FIG. 8. (Color online) QC slab model showing the separations based on common local geometries in the H1 and B1 approximant models and the QC slab. Five groups are identified. Ni and Co atoms; Al-A: cluster of five Al atoms surrounded by five TM atoms; Al-B: cluster of three Al atoms surrounded by TM atoms; Al-C: the remaining Al atoms. Two pentagonal tiles corresponding to the Al-A and Al-B clusters are used to tile the entire QC slab.

parameters in the calculation was lower. The Pendry R-factor for this analysis improved to 0.28. Additional calculations were made to allow two different levels for the Ni atoms (suggested by the H1 approximant structure) but this did not lead to better agreement. This is probably because the relative interlayer locations of the TM atoms are different in the H1 and QC models. The optimized structure is shown in Fig. 9, where the correlations of locations of transition-metal atoms across the layers can be easily observed, along with the other structural features. The optimized parameters from this analysis are given in Tables IX and X. As for the other models, the locations of the TM atoms generally are more precisely known than those of the Al atoms.

We note that two recent studies using STM and other techniques have identified the surface structure of Al-Ni-Co as a random tiling instead of a perfect quasicrystal tiling.[33,34] The approximant models used in this study are consistent

TABLE X. Average interlayer spacings dz and intralyer bucklings Δ for the best-fit structure for the final structure. The corresponding Pendry R-factor is given on the last line.

Parameter	QC model 2 (Å)
dz_{12} (average)	1.90±0.13
dz_{23} (average)	2.03±0.14
dz_{34} (average)	2.0±0.2
dz_{45} (average)	2.1±0.2
dz_{56} (average)	2.0±0.02
dz_{bulk}	2.04
Δ_1 (average)	0.08±0.12
Δ_2 (average)	0.04±0.14
Δ_3 (average)	0.0±0.2
Δ_4 (average)	0.1±0.2
Δ_5 (average)	0.0±0.2
R_P	*0.28*

the reflection symmetries in the H1 and B1 structures allowed a significant increase over the number of parameters that could be varied in those calculations compared to the H2 structure, even allowing for the fact that the H2 unit cell is larger.

The utility of this method is that it allows a fairly rapid way to assess the overall level of agreement between the model and the experimental data, and it also gives a good indication of the nature of the buckling of the layers. If desired, this information can then be usefully applied to determine how to separate the layers in the QC structure model to obtain optimal agreement. In the case presented here, the Pendry R-factor improved from 0.32 to 0.28. More layers could be relaxed, while the number of adjustable parameters

in the calculation was reduced from 26 to 25. Additional features, such as incorporating layers of different compositions or introducing random tiling, may lead to a better agreement. First-principles or semiempirical calculations for the surface structures would be a useful adjunct to these calculations for assessing the stability of the various models.

*Present address: Department of Applied Physics, Stanford University, Stanford CA 94305.

[1] R. McGrath, J. Ledieu, E. J. Cox, and R. D. Diehl, J. Phys.: Condens. Matter **14**, R119 (2002).

[2] R. D. Diehl, J. Ledieu, N. Ferralis, A. W. Szmodis, and R. McGrath, J. Phys.: Condens. Matter **15**, R63 (2003).

[3] M. Gierer and H. Over, Z. Kristallogr. **214**, 14 (1999).

[4] M. Gierer, M. A. Van Hove, A. I. Goldman, Z. Shen, S.-L. Chang, P. J. Pinhero, C. J. Jenks, J. W. Anderegg, C.-M. Zhang, and P. A. Thiel, Phys. Rev. B **57**, 7628 (1998).

[5] N. Ferralis, K. Pussi, E. J. Cox, M. Gierer, J. Ledieu, I. R. Fisher, C. J. Jenks, M. Lindroos, R. McGrath, and R. D. Diehl, Phys. Rev. B **69**, 153404 (2004).

[6] M. A. Van Hove, W. H. Weinberg, and C.-M. Chan, *Low-Energy Electron Diffraction: Experiment, Theory and Surface Structure Determination* (Springer-Verlag, Berlin, 1986).

[7] C. M. Wei, S. Y. Tong, H. Wedler, M. A. Mendez, and K. Heinz, Phys. Rev. Lett. **72**, 2434 (1994).

[8] C. Janot, *Quasicrystals: A Primer* (Clarendon, Oxford, 1992).

[9] A. I. Goldman, J. W. Anderett, M. F. Besser, S.-L. Chang, D. W. Delaney, C. J. Jenks, M. J. Kramer, T. A. Lograsso, D. W. Lynch, R. W. McCallum, J. E. Shield, D. J. Sordelet, and P. A. Thiel, Am. Sci. **84**, 230 (1996).

[10] A.-P. Tsai, A. Inoue, and T. Matsumoto, Mater. Trans., JIM **30**, 463 (1989).

[11] T. Gödecke and M. Ellner, Z. Metallkd. **87**, 854 (1996).

[12] T. Gödecke and M. Ellner, Z. Metallkd. **88**, 382 (1997).

[13] M. Scheffer, T. Gödecke, R. Lück, S. Ritsch, and C. Beeli, Z. Metallkd. **89**, 270 (1998).

[14] S. Ritsch, C. Beeli, H.-U. Nissen, T. Gödecke, M. Scheffler, and R. Lück, Philos. Mag. Lett. **78**, 67 (1998).

[15] S. Ritsch, C. Beeli, H.-U. Nissen, T. Gödecke, M. Scheffer, and R. Lück, Philos. Mag. Lett. **74**, 99 (1996).

[16] K. Saitoh, K. Tsuda, M. Tanaka, K. Kaneko, and A.-P. Tsai, Jpn. J. Appl. Phys., Part 2 **36**, L1400 (1997).

[17] Y. Yan, S. J. Pennycook, and A.-P. Tsai, Phys. Rev. Lett. **81**, 5145 (1998).

[18] E. Abe, K. Saitoh, H. Takakura, A.-P. Tsai, P. J. Steinhardt, and H. C. Jeong, Phys. Rev. Lett. **84**, 4609 (2000).

[19] W. Steurer, T. Haibach, B. Zhang, S. Kek, and R. Lück, Acta Crystallogr., Sect. B: Struct. Sci. **49**, 661 (1993).

[20] H. Takakura, A. Yamamoto, and A.-P. Tsai, Acta Crystallogr., Sect. A: Found. Crystallogr. **A57**, 576 (2001).

[21] P. J. Steinhardt, H. Jeong, K. Saitoh, M. Tanaka, E. Abe, and A.-P. Tsai, Nature (London) **396**, 55 (1998).

[22] K. Saitoh, K. Tsuda, and M. Tanaka, J. Phys. Soc. Jpn. **67**, 2878 (1998).

[23] A. Yamamoto and S. Weber, Phys. Rev. Lett. **78**, 4430 (1997).

[24] P. Gummelt and C. Bandt, Mater. Sci. Eng., A **294-296**, 150 (2000).

[25] P. Gummelt, Geom. Dedic. **62**, 1 (1996).

[26] A. Cervellino, T. Haibach, and W. Steurer, Acta Crystallogr., Sect. B: Struct. Sci. **58**, 8 (2002).

[27] O. Zaharko, C. Meneghini, A. Cervellino, and E. Fischer, Eur. Phys. J. B **19**, 207 (2001).

[28] C. L. Henley, M. Mihalkovic, and M. Widom, J. Alloys Compd. **342**, 221 (2002).

[29] M. Mihalkovic, I. Al-Lehyani, E. Cockayne, C. L. Henley, N. Moghadam, J. A. Moriarty, Y. Wang, and M. Widom, Phys. Rev. B **65**, 104205 (2002).

[30] P. Ebert, F. Kluge, M. Yurechko, B. Grushko, and K. Urban, Surf. Sci. **523**, 298 (2003).

[31] M. Kishida, Y. Kamimura, R. Tamura, K. Edagawa, S. Takeuchi, T. Sato, Y. Yokoyama, J. Q. Guo, and A.-P. Tsai, Phys. Rev. B **65**, 94208 (2002).

[32] E. Cox, J. Ledieu, R. McGrath, R. D. Diehl, C. J. Jenks, and I. Fisher, in *Quasicrystals: Preparation, Properties and Applications*, edited by E. Belin-Ferre, P. A. Thiel, A-P. Tsai, and K. Urban, Materials Research Society Symposium Proceedings Vol. 643 (MRS, Warrendale, 2001), p. 40310.

[33] H. R. Sharma, K. J. Franke, W. Theis, A. Riemann, S. Fölsch, P. Gille, and K.-H. Rieder, Phys. Rev. B **70**, 235409 (2004).

[34] J. Yuhara, J. Klikovits, M. Schmid, P. Varga, Y. Yokoyama, T. Shishido, and K. Soda, Phys. Rev. B **70**, 024203 (2004).

[35] M. Gierer, A. Mikkelsen, M. Gräber, P. Gille, and W. Moritz, Surf. Sci. Lett. **463**, L654 (2000).

[36] I. R. Fisher, M. J. Kramer, Z. Islam, A. R. Ross, A. Kracher, T. Weiner, M. J. Sailer, A. I. Goldman, and P. C. Canfield, Philos. Mag. B **79**, 425 (1999).

[37] L. E. Davis, N. C. MacDonald, P. W. Palmberg, G. E. Riach, and R. E. Weber, *Handbook of Auger Electron Spectroscopy* (Perkin-Elmer, Eden Prairie, 1978).

[38] S. L. Chang, W. B. Chin, C.-M. Zhang, C. J. Jenks, and P. A. Thiel, Surf. Sci. **337**, 135 (1995).

[39] W. Moritz, J. Phys. C **17**, 353 (1984).

[40] J. B. Pendry, J. Phys. C **13**, 937 (1980).

[41] K. Niizeki, J. Phys. A **24**, 3641 (1991).

[42] H. R. Sharma, in *Physics* (Freie University, Berlin, 2002).

[43] W. Steurer, Z. Kristallogr. **190**, 179 (1990).

[44] W. Steurer and T. Haibach, in *The Physics of Quasicrystals*, ed-ited by Z. M. Stadnik (Springer, Heidelberg, 1999), p. 51.

[45] W. Steurer and T. Haibach, in *International Tables for Crystal-lography*, edited by U. Shmueli (Kluwer Academic Publishers, Dordrecht, 2001), p. 486.

[46] M. A. Van Hove, W. Moritz, H. Over, P. J. Rous, A. Wander, A. Barbieri, N. Materer, U. Starke, and G. A. Somorjai, Surf. Sci. Rep. **19**, 191 (1993).

[47] A. Barbieri and M. A. Van Hove (private communication).